



LAWRENCE  
LIVERMORE  
NATIONAL  
LABORATORY

# DETERMINING CORRECT LOCATION OF INTERFACES IN X-RAY IMAGES

Bernard Kozioziemski

October 12, 2004

## **Disclaimer**

---

This document was prepared as an account of work sponsored by an agency of the United States Government. Neither the United States Government nor the University of California nor any of their employees, makes any warranty, express or implied, or assumes any legal liability or responsibility for the accuracy, completeness, or usefulness of any information, apparatus, product, or process disclosed, or represents that its use would not infringe privately owned rights. Reference herein to any specific commercial product, process, or service by trade name, trademark, manufacturer, or otherwise, does not necessarily constitute or imply its endorsement, recommendation, or favoring by the United States Government or the University of California. The views and opinions of authors expressed herein do not necessarily state or reflect those of the United States Government or the University of California, and shall not be used for advertising or product endorsement purposes.

This work was performed under the auspices of the U.S. Department of Energy by University of California, Lawrence Livermore National Laboratory under Contract W-7405-Eng-48.

*Target Area Technologies Program*

*Mail Station L - 472*

*Ext: 4-6317*

September 30, 2004

MEMORANDUM

**TO: Distribution**

**FROM: Bernard Kozioziemski**

**SUBJECT: Determining correct location of interfaces in x-ray images**

---

I. SUMMARY

X-ray phase-contrast enhanced imaging enables characterization of objects otherwise transparent to x-rays. Such imaging is accomplished with a point-source or plane-wave x-rays and in the simplest implementation takes advantage of the refraction of x-rays at interfaces to provide contrast. The refraction of x-rays, while small, can lead to measurable displacements of interfaces in the image plane. A simple approximate analytical expression is obtained for the required correction. The resulting expression is verified with a full raytrace calculation.

II. INTRODUCTION

Advances in micro-focus x-ray sources and synchrotron imaging has enabled phase-contrast methods for x-rays in many applications. NIF ignition targets can be characterized by phase-contrast methods as was recently demonstrated in a collaboration between NIF and Engineering divisions. Phase-effects are always present in x-ray characterizations, even when not specifically used in imaging. The refractive nature of objects, while very weak at x-ray wave-lengths, will shift the apparent position of features in an object as observed in an image. This shift needs to be correctly determined for accurate dimensional characterization of objects. This memo outlines a simple approximation for spherical objects to translate the position of a feature in the image plane to its real position in the object plane.

Figure 1 shows the geometry of the problem. X-rays enter the spherical object from the left and are refracted at each interface. For simplicity, parallel rays are assumed, with the

extension to a point source discussed later. The concentric spherical surfaces bound different materials and x-rays will be refracted at each interface. Once the x-ray leaves the shells, it will travel at angle  $\phi_i$  to the detector a distance  $\Delta z$  from the center of the sphere. The offset  $\Delta\rho$  of the ray at the detector from its incident position can be determined once  $\phi_i$  is known.

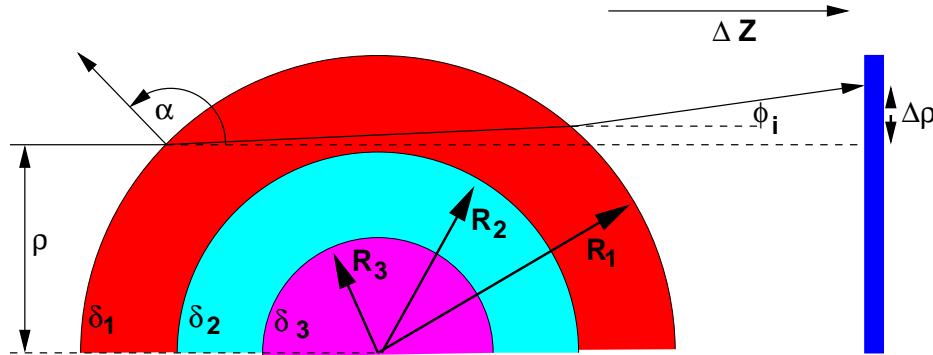


FIG. 1: Geometry of the problem. A ray enters a distance  $\rho$  from the center of the concentric spheres. The ray is refracted at each interface where the real part of the refractive index is  $1-\delta_i$ . After leaving the sphere, it travels a distance  $\Delta z$  to the detector.

The absorption will be neglected in this calculation since it does not contribute to the deflection of the x-rays. Each material is characterized by the real-part of the refractive index, commonly written as  $n_i = 1 - \delta_i$ , where  $i$  denotes each material in the problem and  $\delta \ll 1$ . Since  $\delta$  is small, the x-rays are deflected by a small amount, allowing approximations to the problem.

### III. CALCULATION

Consider first a solid sphere of one material but with a “feature” inside located at radial position  $\rho$  from the center. We want to determine the offset of the feature in the image plane with respect to its position in the sphere,  $\Delta\rho$  in Fig. 1. The ray starting at  $\rho$  intersects the sphere at position  $z = -\sqrt{R_1^2 - \rho^2}$ . The surface normal for the sphere is given by  $\alpha = \arctan(\rho/z) = \arctan(-\rho/\sqrt{R_1^2 - \rho^2})$ . The angle of incidence is  $\theta = \alpha - 0$  for parallel rays. Using Snell’s law,

$$\begin{aligned} \theta_1 &= \arcsin\left(\frac{n_0}{n_1} \sin(\theta_0)\right) \\ &= \arcsin\left(\frac{1}{1 - \delta_1} \sin(\theta_0)\right) \end{aligned}$$

$$\approx \arcsin((1 + \delta_1) \sin(\theta_0)). \quad (1)$$

A Taylor expansion of  $\arcsin((1 + \delta_1) \sin(\theta_0))$  about  $\delta_1 = 0$  gives

$$\begin{aligned} \arcsin(\sin(\theta_0) + \delta_1 \sin(\theta_0)) &\approx \arcsin(\sin(\theta_0)) + \frac{\delta_1 \sin(\theta_0)}{\sqrt{1 - \sin(\theta_0)^2}} \\ &\approx \theta_0 + \delta_1 \frac{\sin(\theta_0)}{\cos(\theta_0)} \\ &\approx \theta_0 + \delta_1 \tan(\theta_0) \\ \theta_1 &\approx \theta_0 + \delta_1 \frac{-\rho}{\sqrt{R_1^2 - \rho^2}}. \end{aligned} \quad (2)$$

This is the refracted angle. The ray travels in the direction of  $\phi_1 = \alpha - \theta_1$ , so the deflected angle is

$$\phi_1 = \delta_1 \frac{\rho}{\sqrt{R_1^2 - \rho^2}}. \quad (3)$$

The ray then proceeds to the other side of the sphere where it is refracted again. Because the deflected angle is small, on the order of  $10^{-5}$  radians, it is a very good approximation to simply take the second point the ray hits at the same  $\rho$  from above. In this case, the deflection after leaving the sphere is simply double that calculated in Eq. 3. Thus for a detector placed a distance  $\Delta z$  from the sphere, the position for this ray will be offset from  $\rho$  by

$$\begin{aligned} \Delta\rho &= 2 \tan(\phi_1) \Delta z \\ &\approx \frac{2\delta_1 \Delta z \rho}{\sqrt{R_1^2 - \rho^2}} \end{aligned} \quad (4)$$

Thus the deflection depends on the radius of the sphere and material property in a simple expression.

The formulation for multiple spherical surfaces is similar at the level of approximation used above. Since the rays are only weakly deflected at each surface, the same impact parameter  $\rho$  can be used for each surface. The deflections at each surface will add to that of the previous surface. Following the above formulation, the deflection of rays passing through two spherical surfaces is

$$\Delta\rho = 2\Delta z \left( \delta_1 \frac{\rho}{\sqrt{R_1^2 - \rho^2}} + (\delta_2 - \delta_1) \frac{\rho}{\sqrt{R_2^2 - \rho^2}} \right). \quad (5)$$

This process is repeated for each of the  $N$  interfaces the ray passes through, giving

$$\Delta\rho = 2\rho\Delta z \sum_{i=1}^N \frac{(\delta_i - \delta_{i-1})}{\sqrt{R_i^2 - \rho^2}}, \quad (6)$$

where  $\delta_0 = 0$  is the vacuum.

The analysis can also be extended to point-projection microscopes when the maximum incident angle is not too large. For a point source a distance  $d_1$  and detector  $d_2$  from the object, the equivalent plane-wave propagation distance is  $\Delta z_{\text{eff}} = \frac{d_1 d_2}{d_1 + d_2}$ .

#### IV. EXAMPLES

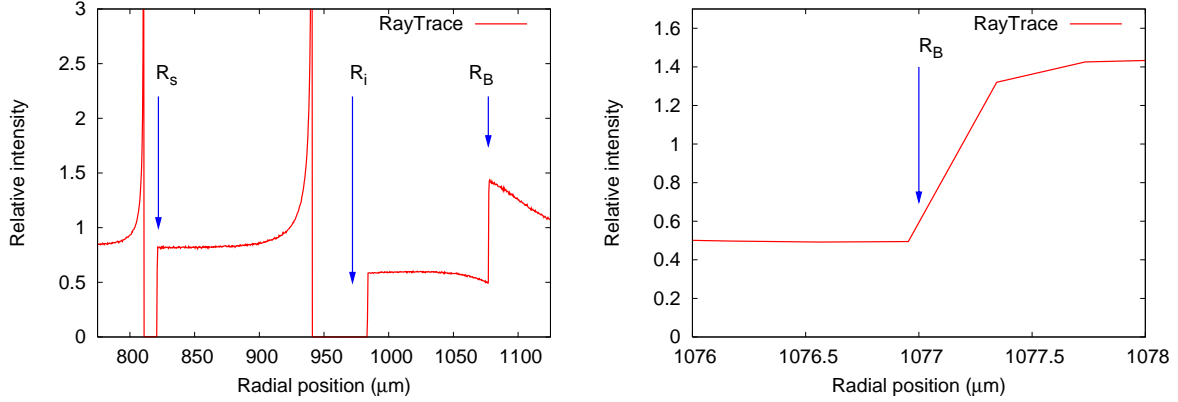


FIG. 2: Raytraced 105  $\mu\text{m}$  wall Be capsule with 150  $\mu\text{m}$  thick DT solid inside. X-ray energy of 8 keV is assumed and the detector distance  $\Delta z$  is 490 mm. The left image shows the full region of interest while the right is near the outer Be shell radius. The blue arrows mark the interfaces as defined in the model.

The calculation is compared to computational raytrace results to verify its validity. A solid D-T layer inside of a beryllium shell was used as the test problem. The Be shell has outer radius  $R_B$  of 1077  $\mu\text{m}$  and inner radius  $R_i = 972 \mu\text{m}$ . The D-T solid has an inner surface with radius of  $R_s = 822 \mu\text{m}$ . The material properties are  $\delta_{\text{Be}} = 5.6\text{e-}6$  and  $\delta_{\text{DT}} = 6.5\text{e-}7$ , appropriate for 8 keV x-rays. Vacuum is assumed outside the Be shell.  $\Delta z$  is set to 490 mm and the detector pixel size is 0.39  $\mu\text{m}$  to clearly demonstrate the interface movement.

Each interface corresponds to a dark band in the image due to the strong refraction of the x-rays passing nearly tangent to the surface. The x-rays at the outer edge of the dark band are those passing just outside the radius of a spherical surface. Thus the outer edge will be slightly offset in the image according to Eq. 4. The interface  $R_i$  is expected to shift by 11.5  $\mu\text{m}$  using Eq. 4 and  $R_s$  is expected to shift -1.2  $\mu\text{m}$  using Eq. 5.

Figure 2 shows the raytrace result covering all the interfaces and close to  $R_B$ . The edge at

$R_B$  is not expected to shift because those rays passing the outside surface are not refracted. Figure 3 shows the raytrace result close to  $R_i$  and  $R_s$ . The surface position in the model is shown with the blue arrow marking  $R_i$  and  $R_s$  respectively. The predicted surface according to Eq. 4 is shown with the magenta arrow. The raytrace results agree well with Eq. 4.

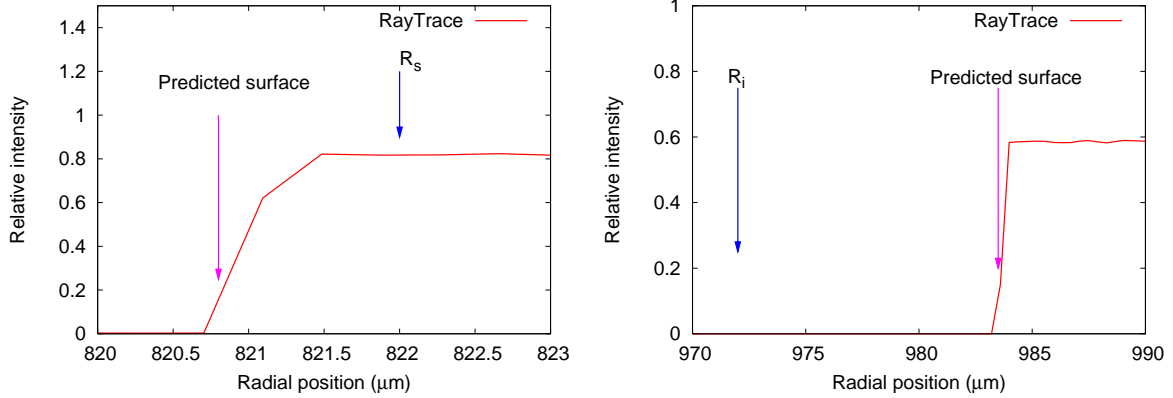


FIG. 3: Raytraced 105  $\mu\text{m}$  wall Be capsule with 150  $\mu\text{m}$  thick DT solid inside. The left image is near  $R_s$  and the right is near  $R_i$ . The blue arrows mark the interface as specified in the raytrace model while the magenta arrow shows the position as calculated from Eq. 5 and Eq. 4 for the left and right images respectively.

## V. CALCULATING THE CAUSTIC POSITION

The above calculation shows the position of the outer edge, that which is effectively obscured by the refraction. The edge described above is not the strongest interface feature. Rather, the strong intensity increase is associated with the the caustic. The position of the caustic in an image can be determined using calculations in Landen's memo[1]. The width of the fringe is subtracted from the edge as determined using Eq. 4 to give the caustic position. Using the geometry in Fig. 1, Landen's expression for the width of the dark band at  $R_i$  is

$$i_c = 3 \left( \Delta z (\delta_{Be} - \delta_{DT}) \sqrt{R_i/2} \right)^{2/3}. \quad (7)$$

The predicted caustic position is compared to the raytrace results. For the cases shown in the figures, the predicted caustic position is 940.9  $\mu\text{m}$ , while in the raytrace the edge appears at 941  $\mu\text{m}$  for  $R_i$ . The DT solid-vapor interface is predicted to be at 810.4  $\mu\text{m}$ , while it appears

at 810.9  $\mu\text{m}$  in the raytrace model. The small difference is likely due to the refraction of the caustic at the outer capsule surface.

## VI. COMPARISON TO FRESNEL PROPAGATION

For the large  $\Delta z$  in the examples, diffraction plays a significant role. The diffraction is often smoothed in experiments because of the source size and detector resolution. Figures 4 and 5 show a Fresnel calculation convolved with a  $\sigma = 2 \mu\text{m}$  Gaussian along with the raytrace results. Also included is the raytrace convolved with a Gaussian response. While the position of the edges is nearly identical for all cases, the Fresnel propagation calculation has a significantly different shape. The peak–valley difference in intensity is considerably smaller than in the raytrace.

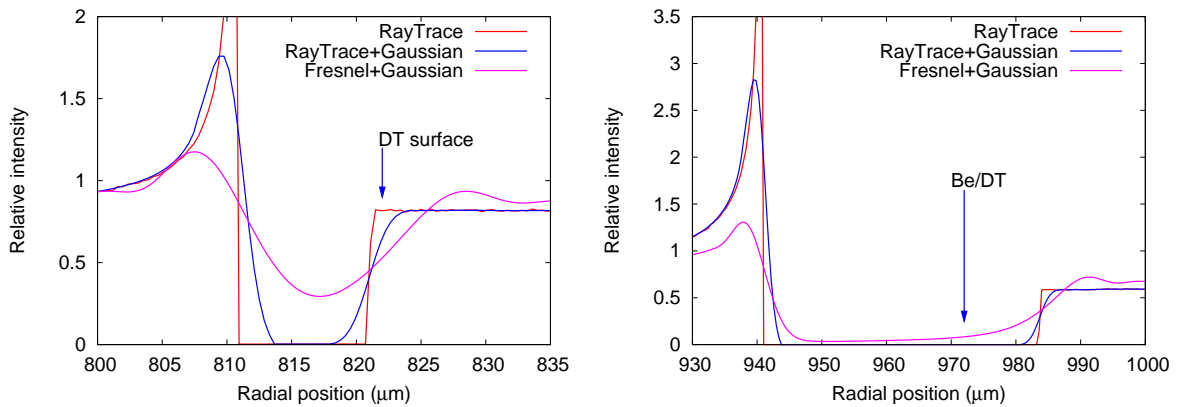


FIG. 4: Comparison of raytrace with no aberrations, raytrace with a Gaussian blurring, and a Fresnel propagation with Gaussian blurring. The left image is near the DT solid–vapor interface and the right is at the DT solid–Be interface. The edges are located at approximately the same position, however there is a significant difference in the shape of the edges using Fresnel propagation.

---

[1] “Refraction Enhanced Imaging from Curved Interfaces”, 2004.

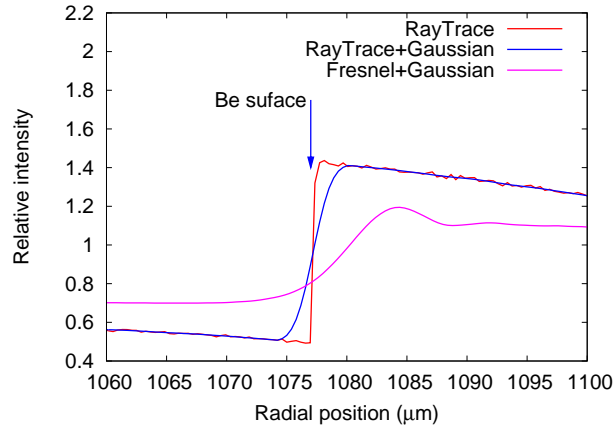


FIG. 5: Comparison of raytrace with no aberrations, raytrace with a Gaussian blurring, and a Fresnel propagation with Gaussian blurring at the outer Be capsule surface.